Journal of the European Ceramic Society 44 (2024) 6124–6134

Contents lists available at ScienceDirect

Journal of the European Ceramic Society

journal homepage: www.elsevier.com/locate/jeurceramsoc

Polymer-derived Biosilicate-C composite foams: In-vitro bioactivity, biocompatibility and antibacterial activity

Fulden Dogrul [a,b,c], Qaisar Nawaz [c], Hamada Elsayed [b,d], Liliana Liverani [c,e], Dušan Galusek [a,f], Enrico Bernardo [b,*], Aldo R. Boccaccini [c,*]

[a] FunGlass – Centre for Functional and Surface Functionalized Glass, Alexander Dubcek University of Trenčín, Trenčín, Slovakia
[b] Department of Industrial Engineering, Università degli Studi di Padova, Padova, Italy
[c] Institute of Biomaterials, University of Erlangen-Nuremberg, Cauerstraße 6, Erlangen 91058, Germany
[d] Department of Glass Research, National Research Centre, Egypt
[e] DGS S.p.A., Rome, Italy
[f] Joint Glass Centre of the IIC SAS, TnU AD and FChFT STU, Centre for Functional and Surface Functionalized Glass, TnUAD, Trenčín, Slovakia

ARTICLE INFO

Keywords:
Biosilicate glass-ceramic
Polymer-derived-ceramics
SiOC
Composites
Antibacterial activity, biocompatibility, cell viability

ABSTRACT

Biosilicate/carbon composites were fabricated in the form of highly porous foams by the polymer-derived ceramic route, and their biological response was analysed. Two different commercial silicone polymers (a poly-methyl-siloxane, MK, and a polymethyl-phenyl-silsesquioxane, H44) were considered as a silica source, mixed with active fillers yielding Na_2O, CaO and P_2O_5. The samples were heat treated either in air or in N_2 atmosphere to obtain products resembling the known Biosilicate® glass-ceramic, with or without free carbon. All fabricated samples exhibited acellular *in-vitro* bioactivity upon immersion in SBF as well as antibacterial activity against *S. aureus* and *E. coli*. Direct contact cell viability test, assessed by using a WST-8 assay, indicated that both carbon-containing and carbon-free samples were cytocompatible.

1. Introduction

Bone defects, resulting from trauma, ageing, tumour resections, malformations, or periodontal disease, represent a serious public health problem [1]. Bone tissue engineering (BTE) aims to satisfy the need for bone grafts, which can replace, repair or regenerate injured, lost, or damaged bone. Three-dimensional structures, named "scaffolds" are considered as the best option for replacing autografts (tissue portions transplanted from one part of the body to another), nowadays known as the gold standard treatment.

The scaffold materials are expected to induce formation of bone [2] under specific conditions. An ideal scaffold must possess some key characteristics such as bioactivity and biocompatibility, controllable degradation rate in the human body during the healing time, and similar mechanical properties to those of host bone [3].

Various research groups have explored many synthetic and natural scaffolds to be used as bone graft substitutes [4]. Among them, synthetic materials are more advantageous due to their easy fabrication and modifiable characteristics, including bio-chemical, physical, and mechanical properties. Synthetic materials, such as polymeric scaffolds, composites, bio-ceramics, bioactive glasses, and glass-ceramics, have been used for bone regeneration or bone reconstruction due to their excellent biocompatibility, biodegradability in addition to remarkable osteoconductivity and osteoinductivity [4,5].

Bioactive ceramics such as hydroxyapatite (HA) [6], bioactive glasses (BGs) [7], calcium phosphates [8] and silicate bio-ceramics [9], have been successfully used for bone tissue engineering applications [10]. However, in the case of bone defects caused by bone tumour surgery, such biomaterials could not fulfil the expectations for the treatment due to possible proliferation of the residual tumour cells [11]. Therefore, it is important to investigate the development and fabrication of a scaffold that can destroy the residual tumour cells prior to tumour recurrence, while simultaneously regenerating the bone to repair large defects.

Photothermal therapy (PTT) utilizes photothermal agents, such as metallic nanostructures (Au-, Ag-, and Cu -based nanoparticles) or carbon nanomaterials (graphene, carbon nanotubes, carbon nanohorns), to generate heat under near infrared light irradiation and consequently destroy tumour cells [12]. Compared to traditional method such as chemotherapy and radiotherapy, PTT allows local therapy with

* Corresponding authors.
E-mail addresses: enrico.bernardo@unipd.it (E. Bernardo), aldo.boccaccini@fau.de (A.R. Boccaccini).

https://doi.org/10.1016/j.jeurceramsoc.2024.03.006
Received 27 July 2023; Received in revised form 15 February 2024; Accepted 4 March 2024
Available online 6 March 2024

minimum invasiveness [13]. Recently, many carbon-based photothermal agents such as carbon dots (CDs) [14] and graphene oxide (GO) [15] have been used in PTT to treat several forms of cancer. For example, beta tricalcium phosphate (β-TCP) scaffolds modified with graphene oxide (GO) were used for bone regeneration and tumour therapy. The GO modified β-TCP scaffolds were obtained by soaking β-TCP into a GO solution [16]. Such functionalized scaffolds destroy tumour cells and stimulate new bone formation at the same time. However, their fabrication method is complicated due to the presence of a secondary treatment for the densification and modification of the photothermal agent, after the manufacturing of bio-ceramic scaffold.

The polymer-derived ceramics (PDCs) route may be a promising alternative since it can yield a carbon phase developed "in-situ", after the heat treatment of polymer precursors in a suitable firing atmosphere [17]. Among preceramic polymers, silicones are known to yield a silica-rich residue; more precisely, in non-oxidative atmosphere, the residue is a silicon oxycarbide (SiOC) ceramic, consisting of silica glass, featuring both Si-O and Si-C bonds, along with free carbon nanosheets [18]. Silica from the thermal transformation of silicones may react with oxide fillers dispersed in the same polymers, forming silicate bioceramics. After firing in an inert atmosphere, the formed silicate phase embeds a secondary carbon phase, applicable in photothermal therapy. So far, investigations about polymer-derived silicate/carbon composites concerned larnite- [11] and forsterite-based systems [19], after extensive filling of silicones with CaO and MgO, respectively. Investigations on multicomponent systems, with silica reacting with many oxides and corresponding to well-established formulations for bone tissue engineering, are still in progress [20].

The CaO-Na_2O-P_2O_5-SiO_2 system is known to comprise the well known 45S5 Bioglass® developed by Hench et al. [21]. Despite the low P_2O_5 content (not exceeding 6 wt%), this glass exhibits extraordinary mineralization capability, with hydroxyapatite formation stimulated by the presence of an amorphous calcium phosphate layer (developed upon ion diffusion from the glass) over a layer of hydrated silica resulting from preliminary interaction between the glass surface and body fluids [22]. Although extensively considered for its excellent bioactivity, 45S5 Bioglass® is limited by its crystallization accompanied by the formation of $Na_2Ca_2Si_3O_9$ which occurs during thermal treatment and impairs viscous flow sintering. The possible improvement of mechanical properties resulting from crystallization is accompanied by some loss of bioactivity [23,24]. Biosilicate® glass-ceramic prepared from the same CaO-Na_2O-P_2O_5-SiO_2 system by a slight modification of the chemical composition of the original 45S5 Bioglass® is recognized as an excellent alternative, since the significant crystallization (with formation of $Na_2CaSi_2O_6$) enhances the mechanical properties, without inhibiting the bioactivity [25,26]. Recent efforts have been dedicated to investigate silicone-based mixtures yielding a Biosilicate®-like semi-crystalline material, containing an extra carbon phase formed by thermal treatment in nitrogen atmosphere [27]. Besides affecting the phase development, the adoption of PDC technology enhances the shaping possibilities, with foams and 3D-printed scaffolds manufactured from precursors before the ceramic conversion. Moreover, polymer-derived Biosilicate-C composite foams have exhibited photothermal effects, with rapid heating up to ~70°C under infrared irradiation. A plateau is reached after approximately 5 min, and the maximum achieved temperature is maintained for approximately 60 seconds after IR lamp shutdown [20]. However, such promising materials undoubtedly require validation in terms of their in-vitro bioactivity, cytocompatibility and antibacterial activity, to represent a real alternative to materials prepared by more conventional methods.

Herein, we report on the biological response of polymer-derived Biosilicate-C composite foams, processed in nitrogen atmosphere, in comparison to carbon-free Biosilicate®-like glass-ceramic foams (treated in air) used as the control. The study includes the investigation of the cellular response of ST-2 stromal cells, of in-vitro apatite formation after immersion in simulated body fluid (SBF) solution and of antibacterial activity against *S. aureus* and *E. coli*.

2. Experimental procedure

2.1. Manufacturing of polymer-derived Biosilicate-C composite glass-ceramic foams

Biosilicate®-like glass-ceramic and Biosilicate-C composite foams were fabricated following the protocol reported in our previous paper [19]. Briefly, two different commercial silicone polymers (a poly-methyl-siloxane, MK, and a polymethyl-phenyl-silsesquioxane, H44, both from Wacker Chemie AG, Munich, Germany) were used as the source of silica. Once silicone polymers were dissolved in isopropyl alcohol (C_3H_8O, 2-Propanol, HPLC BASIC, Scharlau, Scharlab Italia srl, Riozzo di Cerro al Lambro, Italy), they were mixed with the fillers, which served as the sources of Na_2O, CaO, and P_2O_5, until obtaining an agglomerate-free suspension. The samples were foamed at a low temperature (< 350 °C) and heat treated either in air or in N_2 atmosphere to obtain products resembling Biosilicate® glass-ceramic embedded in a silico-phosphate glass matrix with and without free carbon. For simplicity, the foamed samples heat treated in air are in the following text named as MK and H44, depending on the used silicone precursor, whereas the samples treated in N_2 and featuring an extra carbon phase are denoted as MK-C and H44-C.

2.2. Physical and mechanical properties

A digital calliper was used to measure the dimensions of all samples after the heat treatment. A helium pycnometer (Micromeritics AccuPyc 1330, Norcross, GA) was used to determine the apparent and real density of the obtained foams. Microstructural characterization of the samples was carried out by scanning electron microscopy (SEM, FEI Quanta 200 ESEM, Eindhoven, Netherlands), equipped with energy dispersive spectroscopy (EDS).

The samples were subjected to compression tests (Quasar 25, Galdabini, Cardano, Italy), operating at a crosshead speed of 1 mm min^{-1}. Each data point represents an average value obtained by testing at least five specimens.

2.3. In vitro acellular bioactivity

The acellular bioactivity of the Biosilicate®- like and Biosilicate- C composite foams derived from MK- and H44 silicone resin, fired in air or nitrogen atmosphere, was evaluated by immersion in simulated body fluid (SBF), prepared according to Kokubo's method [28]. 37.5 mg of the foams were immersed in 70 mL SBF and incubated under continuous agitation (120 rpm) at 37°C for 1, 3, 7, 14, and 21 days. At every time point the samples were collected and washed with deionized water and dried. The pH of the remaining SBF media was recorded after every time point. Later, the samples were characterized by scanning electron microscope (SEM; Auriga Base, Zeiss) and Fourier Transform Infrared Spectroscopy (FTIR; IR Affinity- IS, Shimadzu) in attenuated total reflectance (ATR) mode, in a wavenumber range of 4000–400 cm^{-1} with a resolution of 4 cm^{-1} with 40 spectral scans. X-ray diffraction analysis using a diffractometer (XRD, Bruker AXS D8 Advance, Bruker, Germany) in the 2θ range of 10° to 70° equipped with Cu Kα radiation was carried out to identify the phase composition before and after the immersion. The phase identification was supported by the Match! program package (Crystal Impact GbR, Bonn, Germany), operating on data from PDF-2 database (ICDD-International Centre for Diffraction Data, Newtown Square, PA).

2.4. In-vitro cell viability assay

Before starting the cell experiments, all foamed samples (0.2 g) were sterilized by heat treatment at 180°C for 3 h in a furnace (Naberthem,

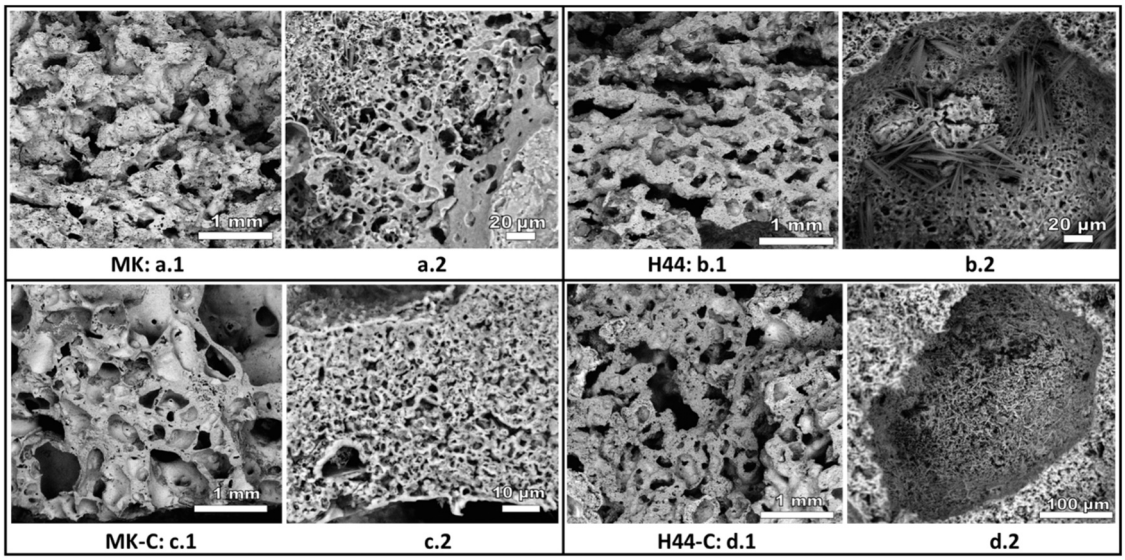

Fig. 1. Microstructural details of polymer-derived Biosilicate-like foams: a: MK; b: MK-C; c: H44; d: H44-C, adapted from Dogrul et al. [20] (with permission from the Editor).

Table 1
Physical and mechanical properties of polymer-derived glass-ceramic foams.

Sample	Geometrical density (g/cm^3)	True density (g/cm^3)	Total porosity (vol %) [ρ_{rel} =1-P_{tot}]	Compressive strength (MPa) [strength-to-density (MPa·g/cm^3)]
MK	0.71 ± 0.06	2.74 ± 0.01	0.74 ± 0.02 [ρ_{rel} = 0.306]	1.2 ± 0.1 [1.7]
MK-C	0.54 ± 0.06	2.63 ± 0.01	0.79 ± 0.02 [ρ_{rel} = 0.205]	1.15 ± 0.03 [2.12]
H44	0.68 ± 0.01	2.70 ± 0.01	0.74 ± 0.01 [ρ_{rel} = 0.256]	1.8 ± 0.1 [2.64]
H44-C	0.55 ± 0.01	2.55 ± 0.01	0.78 ± 0.01 [ρ_{rel} = 0.214]	1.65 ± 0.05 [3]

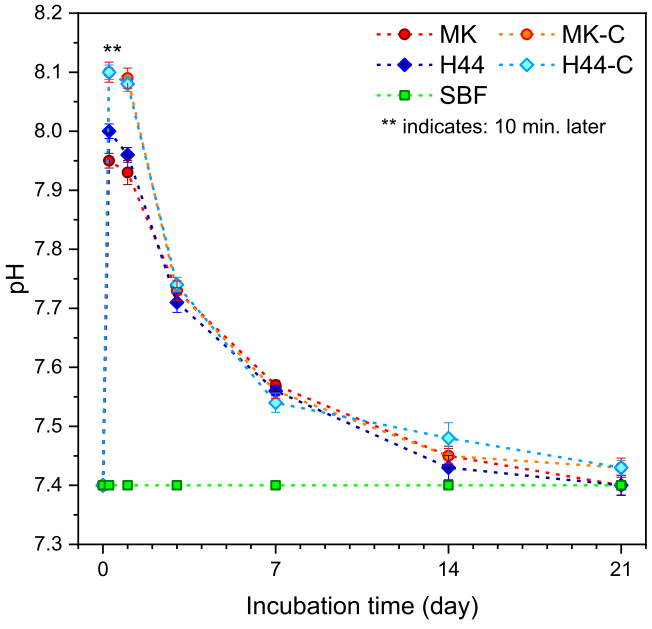

Fig. 2. pH changes of SBF solution containing MK, H44, MK-C and H44-C foams after different immersion times. The initial pH value at 37 °C was 7.4 (error bars indicate the standard deviations).

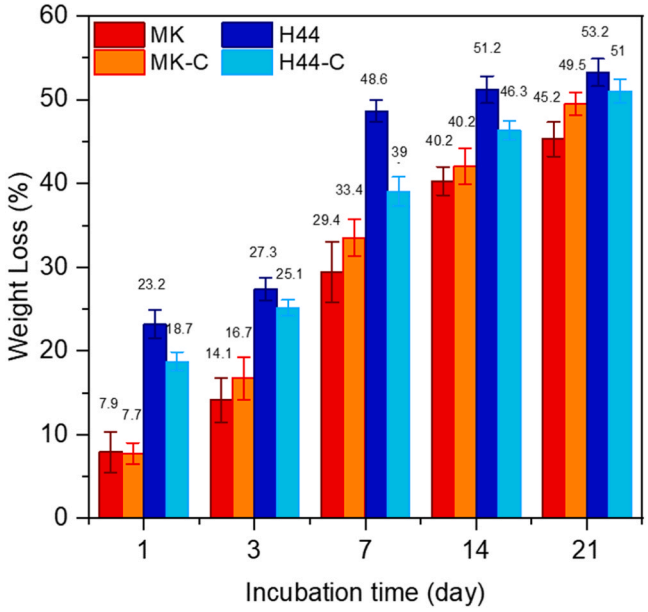

Fig. 3. Weight loss of foams during immersion time (1, 3, 7, 14 and 21 days) in SBF solution at 37 °C (The error bars denote the standard deviation (n = 3, samples in triplicate).

Germany). The samples were then placed in 24 well plates and preconditioned for 7 days in cell culture medium RPMI 1640 (Gibco), containing 10 vol% of fetal bovine serum (FBS, Sigma-Aldrich), and 1 vol% of penicillin/streptomycin (Gibco). Direct contact cell viability test was carried out on foamed samples using ST-2 stromal cells (Leibniz-Institute DSMZ— German Collection of Microorganisms and Cell Cultures GmbH, Germany). The ST-2 cells were maintained in the cell culture medium at 37°C in a humidified atmosphere of 95% air and 5% CO_2 until the cell seeding of the scaffolds. Cell culture medium was removed from the well plates after preconditioning and, subsequently, ST-2 cells were seeded directly on the foamed samples placing a 100 μL drop of cell suspension with an inoculum ratio of 5×10^4 cells/mL and incubating for 15 min to allow the complete soaking of the scaffold. Then the wells were filled with 1 mL of RPMI medium.

Cell viability, after 1 day and 7 days incubation at 37°C in 5% CO_2,

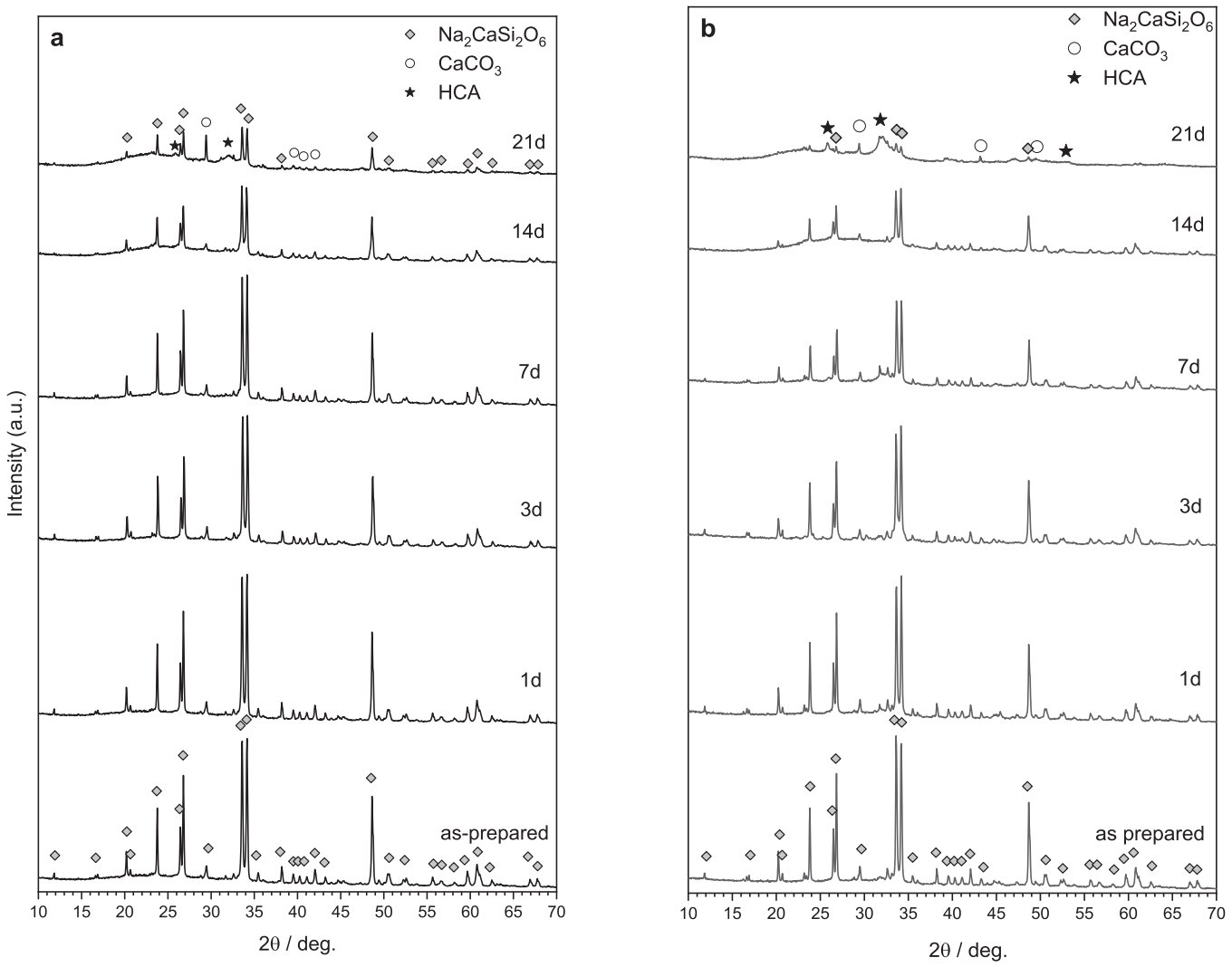

Fig. 4. X-ray diffraction patterns of polymer-derived Biosilicate before and after immersion in SBF solution for 1, 3, 7, 14, and 21 days, a) MK foam and b) H44 foam.

was determined using WST-8 assay ((2-(2-methoxy-4-nitrophenyl)-3-(4-nitrophenyl)-5-(2.4-disulfophenyl)-2 H-tetrazolium, monosodium salt), Sigma). WST-8 is a colorimetric assay that yields orange formazan. The amount of formed formazan is proportional to the number of living cells in the culture. After incubation for 3 h at 37°C, the reaction product was measured at 450 nm using a microplate reader (PHOmo Elisa reader, Autobio Diagnostics Co. Ltd.). Each experiment was carried out in triplicate.

Additionally, rhodamine phalloidin (RP; ThermoFisher Scientific) and DAPI (ThermoFisher Scientific) staining was performed to explore cell adhesion and cell morphology. The staining protocol started with fixation and permeabilization of the adherent cells. Afterwards, rhodamine phalloidin (8 μL/mL) was added and incubated at 37°C for 1 h. Incubated samples were rinsed gently with PBS and dyed by DAPI (1 μL/mL). A fluorescent microscope (Axio Scope A1, Zeiss) was used to analyse the samples.

2.5. Antibacterial activity

The antibacterial activity of foamed samples was determined on *S. aureus* (Gram-positive) and *E. coli* (Gram-negative) bacteria. Firstly, the bacteria strains were incubated in the LB-medium (lysogeny broth, Carl Roth, Germany) at 37°C for 24 h, and the optical density (OD) of the bacteria population was calibrated (600 nm, Thermo Scientific™ GENESYS 30™, Germany) to reach the value of 0.015, according to turbidity measurements of bacterial cultures. Before the antibacterial activity evaluation, the selected samples (0.2 g) were sterilized at 180°C for 3 h. Then, the samples were placed into a tube with 20 μL of bacterial suspension, 2 mL of medium was added, and the OD was measured. The samples were incubated at 37°C for 3, 6 and 24 h. At the given time points (3, 6 and 24 h) aliquots of bacterial suspension were taken out, their optical density was recorded, and relative bacterial viability was calculated using the following equation:

$$\text{Relative Bacterial Viability}(\%) = \frac{\text{Sample OD}}{\text{Control OD}} \times 100 \quad (1)$$

The medium was used as a blank and the bacterial cells suspension was used as the control. Three parallel experiments were performed for each sample.

2.6. Weight loss determination

Weight loss measurements during the studies related to the degradation of the glass-ceramic scaffolds (MK, H44 and MK-C, H44-C) in SBF with the pH 7.4 were carried out at 37.5 °C (in the range of the human body temperature). The sample degradation rate in SBF was estimated by evaluating weight loss of the samples after immersion for different time intervals (1, 3, 7, 14, and 21 days). At every time point, the glass-ceramic scaffolds were removed from SBF, rinsed with deionized water, dried, and weighed. The weight loss of the samples was calculated using

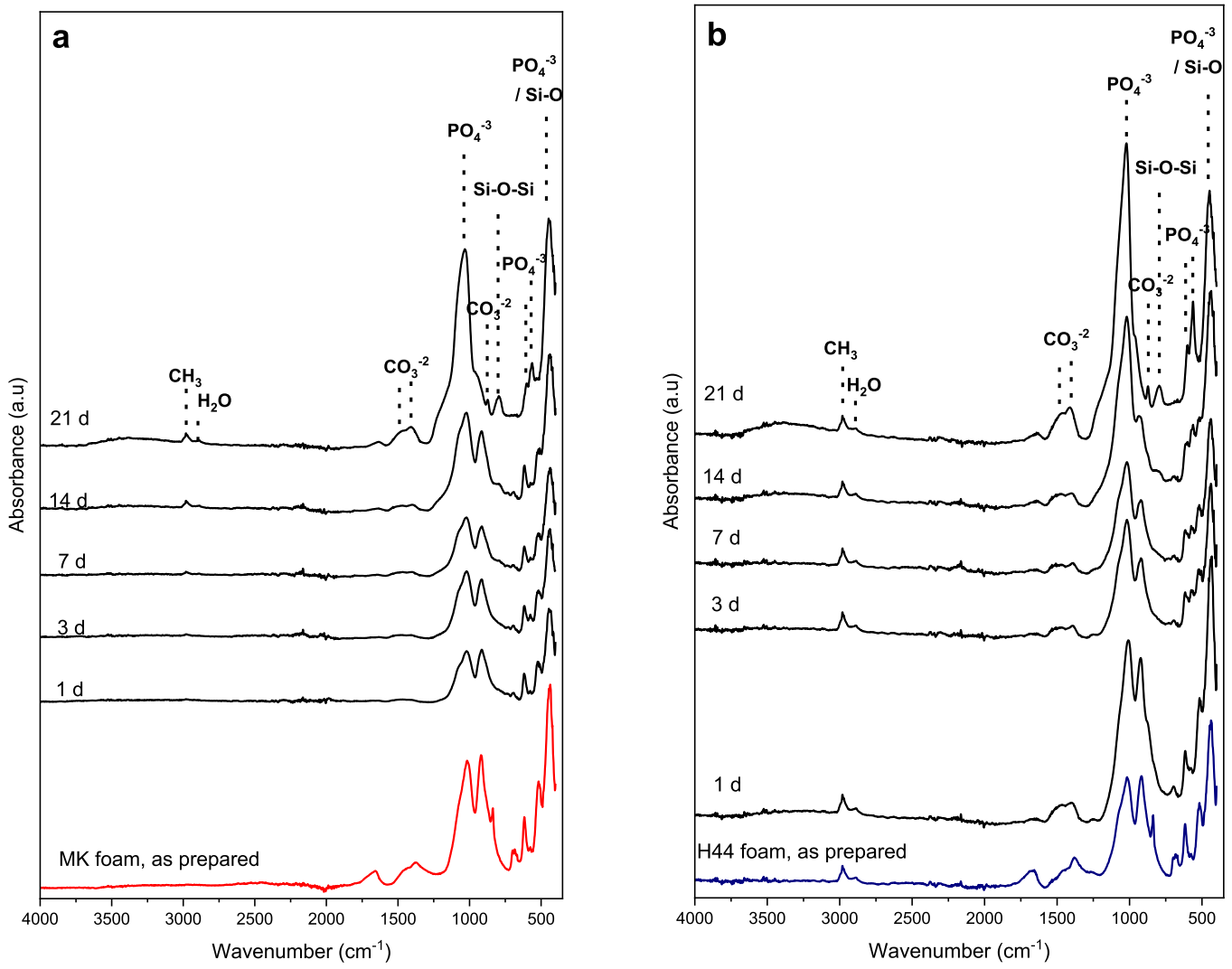

Fig. 5. FTIR spectra of a) MK foam and b) H44 foam after immersion in SBF for 1, 3, 7, 14 and 21 days.

the formula:

$$Weight \quad Loss = \frac{Wo - Wt}{Wo} \times 100 \tag{2}$$

where W_o is the weight before immersion and the W_t is the weight of the sample after a specific time of soaking.

2.7. Statistical analysis

All experiments were carried out at least in triplicate. The results are expressed as the mean ± standard deviation (SD). Statistical evaluation was carried out using one-way analysis of variance (ANOVA) with $p < 0.05$ considered significant.

3. Results and discussion

3.1. Properties of polymer-derived Biosilicate-based foams

The starting point for the present investigation was represented by ceramic foams with hierarchical porosity (Fig. 1), resulting directly from the used precursors, and prepared according to the protocol reported by Dogrul et al. [20]. In particular, macro-porosity developed at a low temperature (< 350 °C), as the result of dehydration of hydrated Na-phosphate. The related water vapour release occurred with the silicones still in polymer state, resulting in significant bloating. Additional porosity resulted from the decomposition of the matrix and the added carbonates at higher temperatures. The crystallization of the typical phase of Biosilicate® glass-ceramics (sodium calcium silicate, $Na_2CaSi_2O_6$) occurred along with the formation of liquid phase from Na-phosphate that, upon cooling, transformed into glass.

The silicone/filler ratios had to be calibrated depending on the different ceramic yield of the two silicone resins (MK and H44), and also with respect to the application of thermal treatment in N_2 atmosphere instead of air. When fired in a non-oxidative atmosphere, silicones do not transform into silica, but into a complex silicone oxycarbide (SiOC) nanocomposite, with variable stoichiometry. According to Scheffler et al. [29], MK silicone resin yields a 31.6%Si-48.1%O-20.2%C (wt%), i.e. $Si_3O_{4.56}C_{1.92}$ ceramic, while H44 transforms into 18.7%Si-28.7%O-52.6%C ($Si_3O_{4.6}C_{8.45}$). The combination with Na_2O-, CaO- and P_2O_5-yielding fillers promoted the separation of the SiOC residues into silica, forming a Biosilicate®-like matrix, and additional carbon-based phases [20].

Table 1 summarizes the physical and mechanical properties of MK, H44, MK-C and H44-C foams. The crushing strength of MK foams (Fig. 1a) did not differ significantly from the previously fabricated foams with a similar, completely open overall porosity (70–75%) [26]. On the other hand, H44 foams (Fig. 1b), exhibited a substantial improvement, visible especially from the strength-to-density ratio. The difference

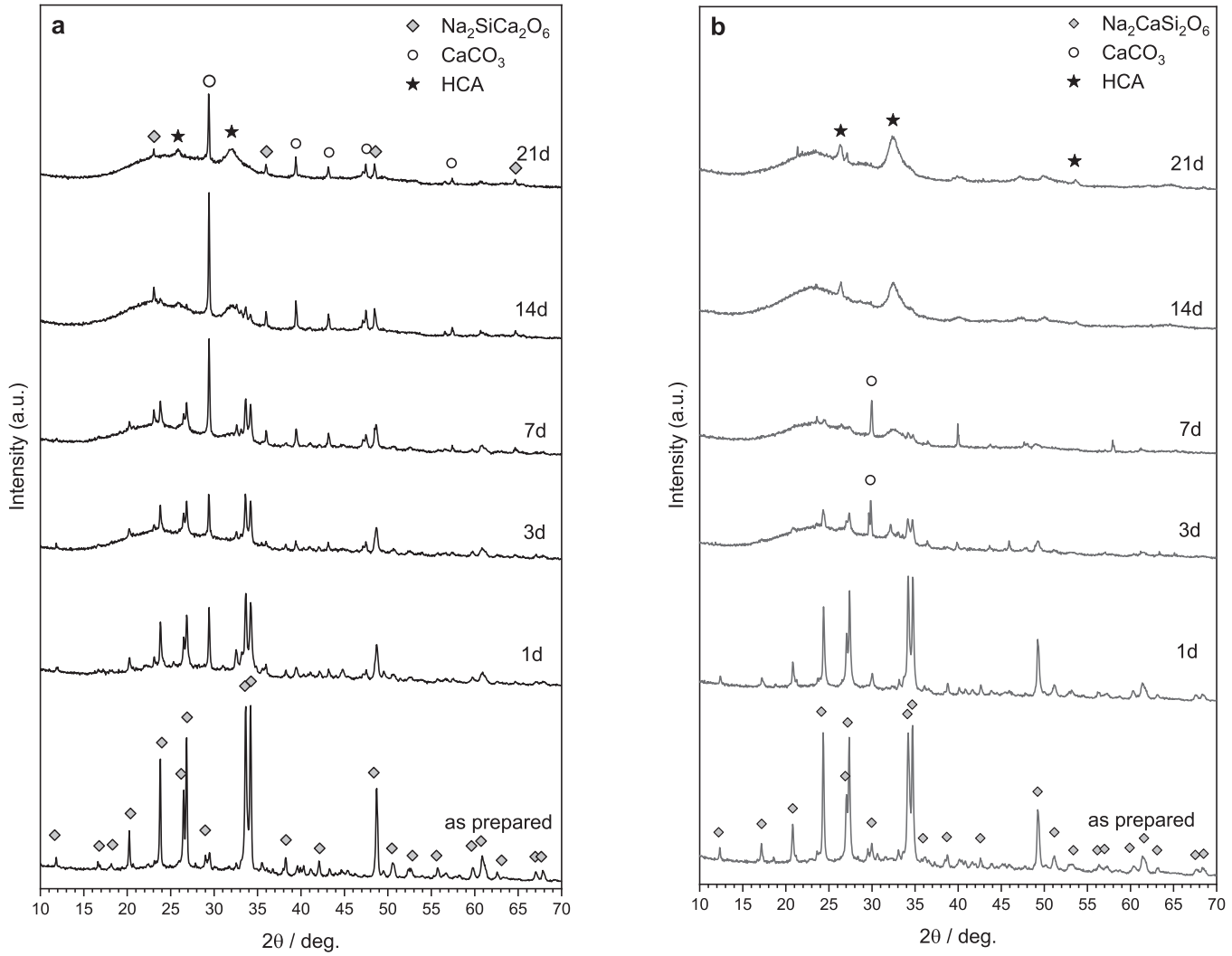

Fig. 6. X-ray diffraction analysis of MK-C and H44-C Biosilicate-C composite foam after immersion in SBF solution for 1,3,7,14 and 21 days.

could not be attributed to a more homogenous cellular structure, since the foams were characterized by quite coarse cell walls (Fig. 1b, left); it could derive from the extensive development of interlocked fibrous crystals inside porous struts (Fig. 1b, right), often protruding from cell walls. A further improvement of strength-to-density ratio was observed for both polymer precursors (MK-C in Fig. 1c; H44-C in Fig. 1d) after firing in N_2. The latter effect was attributed to the well-known reduction of internal stresses during ceramic transformation of silicones in non-oxidative atmosphere [18].

3.2. *In-vitro bioactivity test*

Fig. 2 shows the changes in the pH values of all the produced foams, after immersion in SBF solution for 10 min, 1, 3, 7, 14, and 21 days. A strong increase in pH at the start of the in-vitro bioactivity test was observed, particularly after 10 min (marked with the symbol: **) and 1 day immersion. After 10 min immersion in SBF solution, pH values of MK and H44 foams were 7.95±0.01 and 8.01±0.01 respectively. The pH values of MK-C and H44-C composite foams were even higher (8.09 ±0.01 and 8.08±0.01, respectively). The rise in pH values after immersion of the foams in SBF was attributed to cation (Na^+ and Ca^{2+}) exchange from the glass-ceramics with protons from the SBF solution [30].

As observed in previous in-vivo studies, an alkaline pH does not inhibit bone healing [31]. The pH decreased substantially after 3 days and later stabilized slightly above its initial value (in the range of 7.4–7.6).

The time dependences of weight losses of the MK, H44, MK-C and H44-C foams immersed in SBF solution from 1 to 21 days are shown in Fig. 3. All specimens gradually dissolved during the immersion period. The resulting weight loss indicated that H44-derived foams dissolved faster than the MK-derived ones over the whole soaking period. After 3 days of soaking, a rapid increase in weight loss (48.65%) is observed for the H44 foam. After longer soaking times such as 14 and 21 days, the weight losses recorded for other foams were similar to the weight losses of the H44 Biosilicate foam.

The XRD patterns of MK and H44 foams (fired in air) after immersion in SBF solution for 1, 3, 7, 14, and 21 days are shown in Fig. 4. The diffraction maxima typical of Biosilicate® glass-ceramics (attributed to $Na_2CaSi_2O_6$ [PDF#77–2189]) for MK-derived samples (Fig. 4a) remained visible even after 21 days immersion. However, some dissolution of the main phase was observed, according to the strong decrease in intensity of the diffraction lines after 14 days. An exception is represented by the diffraction maximum at 2θ~30°; this may be justified by the overlapping with the signal from a newly formed phase, namely $CaCO_3$ [calcite, PDF#87–1863]. After 21 days, additional diffraction maxima consistent with carbonated hydroxyapatite (HCA, $Ca_5(PO_4, CO_3)_3(OH)$, PDF#19–0272), were also detected. H44 foams evolved in a similar way, except for longer times: after 21 days, the diffraction lines attributed to $Na_2CaSi_2O_6$ nearly disappeared, with more pronounced

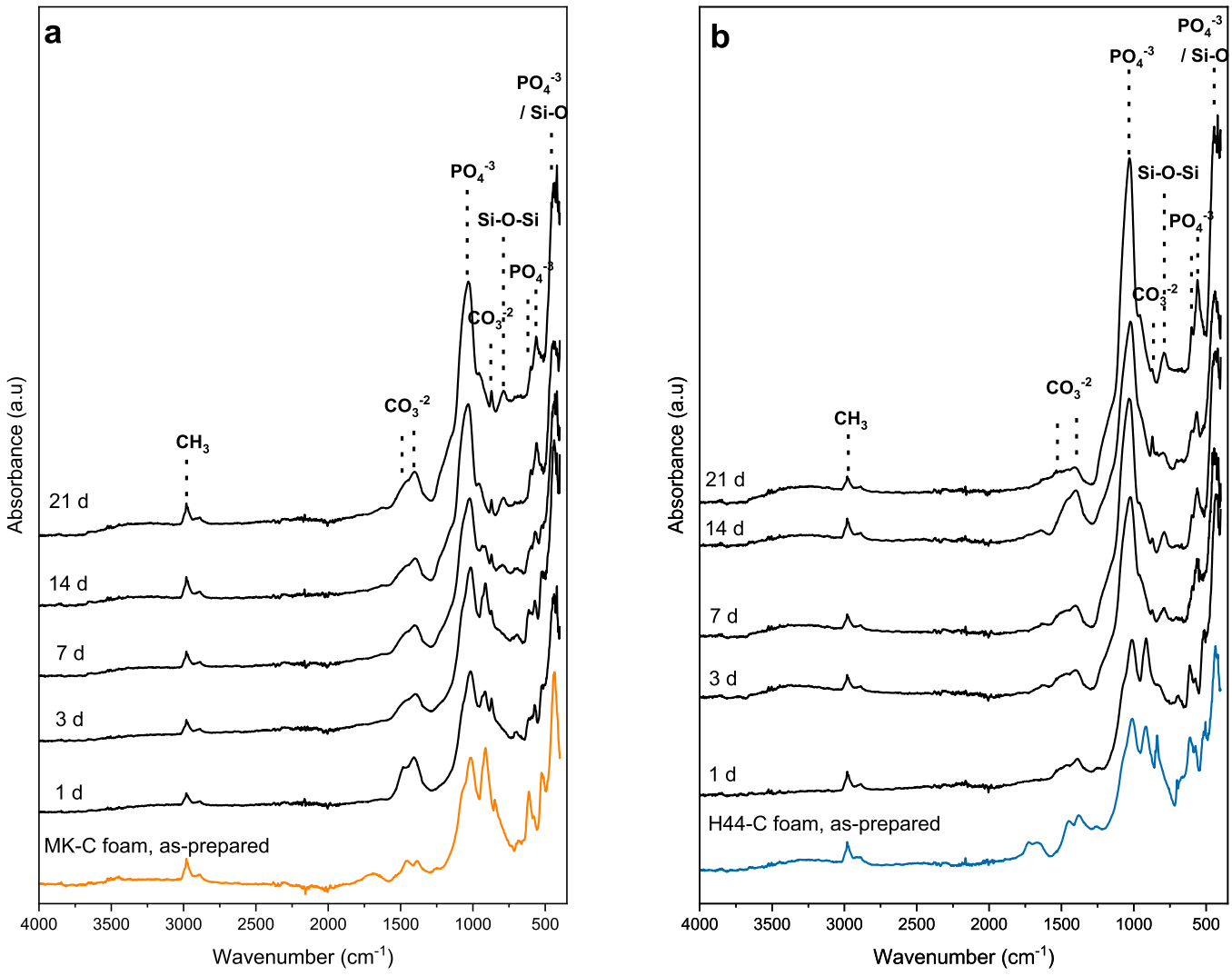

Fig. 7. FTIR spectra of a)MK-C and b) H44-C composite foams and after immersion in SBF for 1,3,7,14 and 21 days.

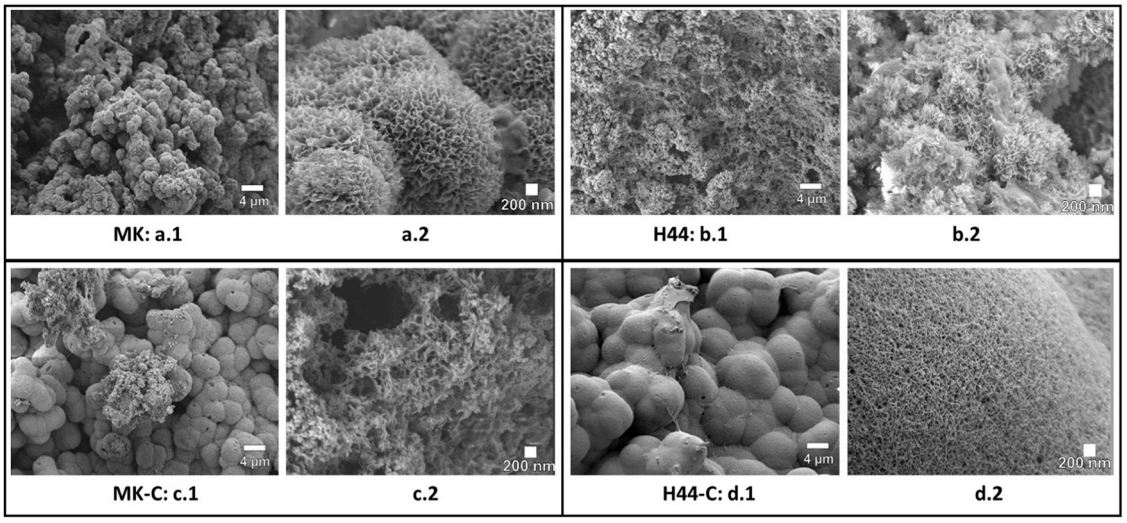

Fig. 8. SEM micrographs of fabricated foams soaked in SBF for 14 days (left: low magnification, right: high magnification): a) MK; b) H44; c) MK-C; d) H44-C.

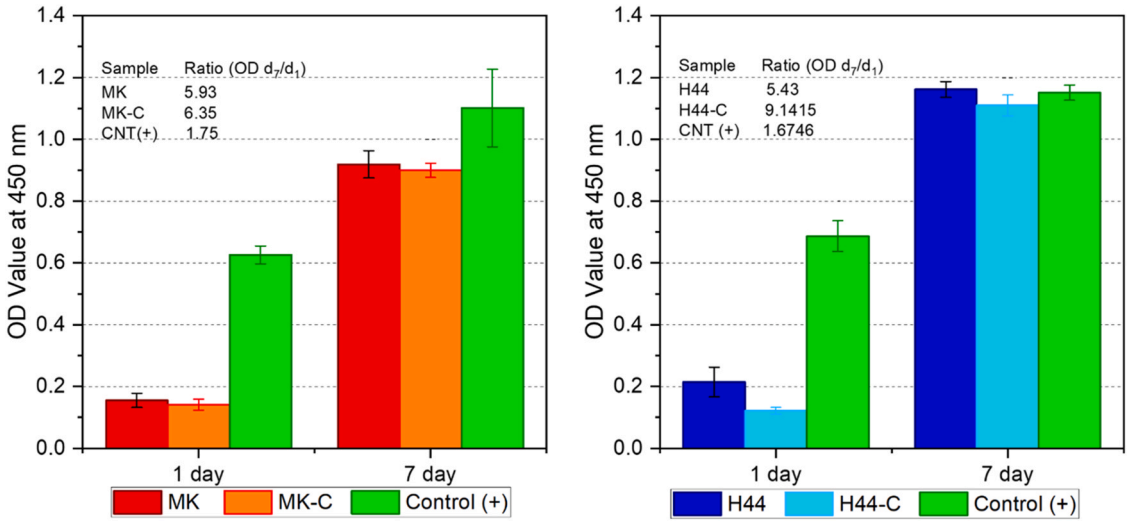

Fig. 9. ST-2 cell viability assessed by WST- 8 assay (OD 450 nm) after direct seeding of cells on MK, MK-C, H44 and H44-C foams (n = 3, samples in triplicate).

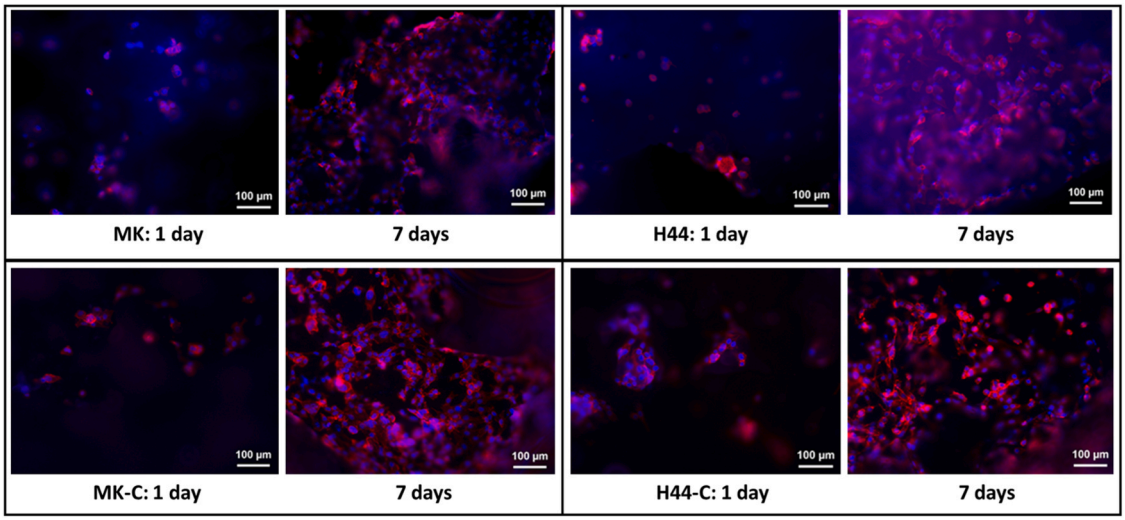

Fig. 10. Fluorescent staining of adherent ST-2 cells on MK- and H44-derived Biosilicate and Biosilicate-C composite foams, after 1 day and 7 days.

HCA-related reflections and $CaCO_3$ still visible as a minor impurity.

The presence of $CaCO_3$ is interesting, in analogy with recent studies on bioactive glasses [32–35]. Mami et al. [32], investigated the surface reactivity of a sol-gel derived bioactive glass with the molar composition of $60SiO_2$-35CaO-5 P_2O_5. They found that the presence of calcium carbonate was not related to the volume of SBF used (i.e. supersaturation of the solution). Calcite nanocrystals could form within the early hours of immersion in SBF due to a fast release of calcium ions from the glass structure and their reaction with hydrogen carbonate anions in the SBF solution. Brauer et al. [35] observed that the phosphate ion concentration is critical: if all available phosphate ions from the glass dissolution are involved in the formation of the apatite phase, the excess calcium ions react with HCO_3^- from dissolved atmospheric CO_2, yielding $CaCO_3$; conversely, a high phosphate ion concentration in SBF solution contributes to the formation of apatite.

It should be noted that calcite is a quite special material, applicable in bone-tissue engineering, as it can bond to bone without forming a surface apatite layer. In fact, the formation of calcite could be an advantage: some reports revealed that calcite could promote better bone marrow induced-osteogenesis than hydroxyapatite scaffolds [36,37].

FTIR spectra of MK and H44 foams in the as-received state and after immersion in SBF solution from 1 to 21 days are shown in Fig. 5. The peaks at approximately 1060 cm^{-1} (P-O stretch), 570, and 600 cm^{-1} (P-O bending), attributable to the formation of crystalline HCA became clearly visible after 21 days for MK foam and after 14 days for H44 foam [38,39]. An additional band at 875 cm^{-1} appearing after 21 days of SBF immersion for MK and H44 foams can be assigned to $\upsilon_2(CO_3^{-2})$ vibrations. Furthermore, the intensity of the $\upsilon_2(CO_3^{-2})$ bands at 1410 and 1500 cm^{-1} (assigned to carbonates) became sharper with increasing SBF immersion time [40].

The XRD patterns of the MK-C and H44-C composite foams before and after immersion in SBF solution are shown in Fig. 6. In MK-C foams, a substantial decrease in intensity of diffraction lines of $Na_2CaSi_2O_6$ was observed after just one day of immersion. A pronounced $CaCO_3$ formation was detected at the early stages of immersion (Fig. 6a). The amount of precipitated $CaCO_3$ increased with increasing immersion time up to 14 days in SBF. However, the intensity of the diffraction maxima of $CaCO_3$ decreased with the increasing HCA formation after 21 days. In MK-C foams, no practical change in the intensity of diffraction maxima of $Na_2CaSi_2O_6$ was observed after 1 day, but the phase nearly disappeared after just 3 days. The formation of $CaCO_3$ in H44-C composite was not as pronounced as for the MK-C composite (Fig. 6b), but was detectable after 1, 3, and 7 days of immersion in SBF. Finally, after 14 days immersion in SBF, HCA remains as the only crystalline phase.

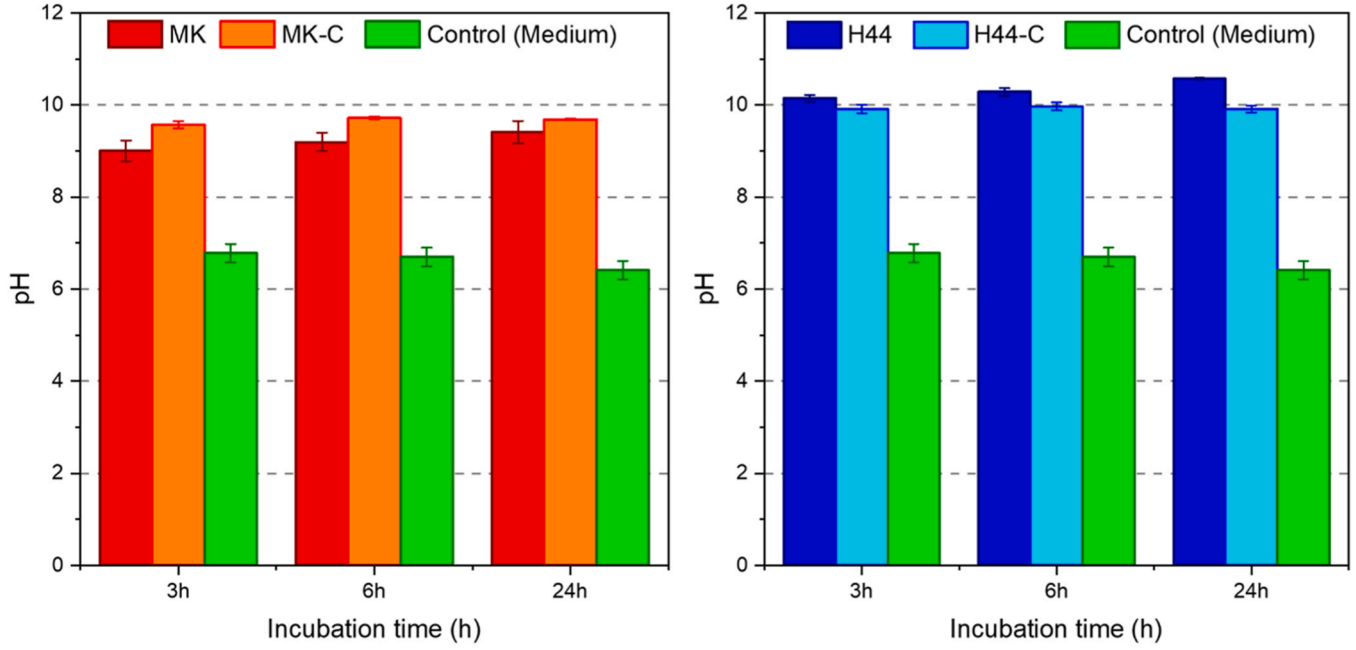

Fig. 11. pH changes in LB medium after immersion of MK, H44, MK-C and H44-C samples (10% w/v) for 3, 6, and 24 h (n = 3, samples in triplicate).

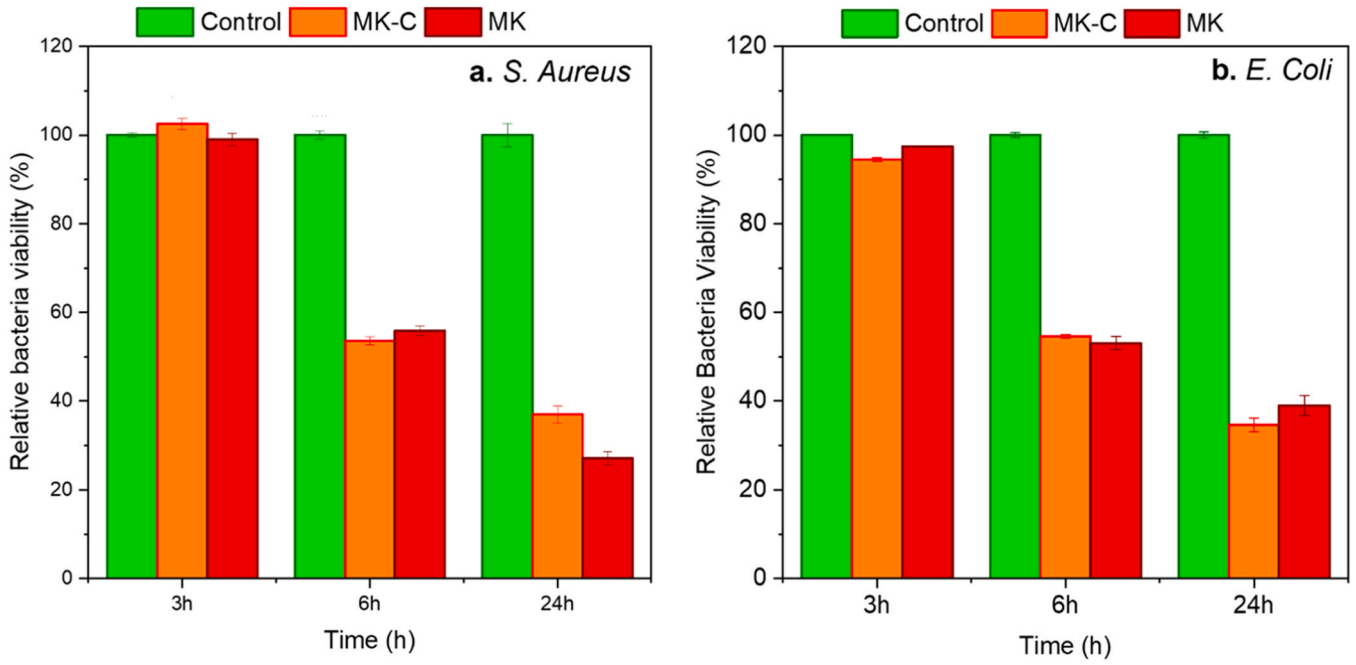

Fig. 12. Antibacterial activity of MK-derived Biosilicate and Biosilicate-C composite foams after 3, 6 and 24 h incubation with a) S. aureus (Gram-positive) and b) E. coli (Gram-negative) bacteria (n = 3, samples in triplicate).

The FTIR spectra of MK-C and H44-C composites foam after 1 day immersion in SBF solution are practically identical in as-received state, except for the intensity of the absorption band at 926 cm^{-1}, which decreased, implying the rapid dissolution of Na^{+} and Ca^{2+} (Fig. 7). The dissolution rate of network-modifying ions (Na^{+} and/or Ca^{2+}) from MK-C composite into SBF was much lower than that from H44-C composite. The small band around 800 cm^{-1}, representing vibrations from amorphous Si-OH silanols at the interface between material and solution, appeared from MK-C composite after 7 days; the same band, from H44-C composite, was more intense after only 3 days incubation.

In parallel, HCA on the H44-C foams was identified at earlier soaking times than on MK-C foams (Fig. 7). More specifically, the formation of crystalline HCA was inferred from the appearance of bands at approximately 1060 cm^{-1} (P-O stretch), 570, and 600 cm^{-1} (P-O bending [41, 42]), after 7 days and 3 days incubation in SBF, for MK-C and H44-C foams, respectively. Bands attributable to carbonate group, $\upsilon_2(CO_3^{-2})$, at ~ 1460, 1420, 875 cm^{-1} appeared after 3 days for H44-C composite, while for MK-C foams they remained hardly visible after 7 days of immersion. The evidence of $CaCO_3$ formation obained by FTIR spectroscopy matched well the results of X-ray diffraction analysis.

In general, carbon containing Biosilicate foams (MK-C and H44-C) exhibited a faster HCA formation compared to foams fabricated in air

(MK and H44 Biosilicate®-like glass ceramics). This could be attributed, in our opinion, to enhanced ion diffusion at interfaces between the silicate matrix and the secondary carbon phase. The mechanism is yet to be understood, but it is known that sodium ions may migrate in carbon-rich domains in SiOC-based anodes for Na-ion batteries, likely due to the wider, irregular spacings compared to graphite [43]. The supporting role of the carbon phase is confirmed by the enhanced reactivity of H44-C foams (having a more abundant carbon phase), compared to MK-C foams [20].

The SEM micrographs of the fabricated foams soaked in SBF for 14 days, presented in Fig. 8, confirm the previous findings. The surface of all foamed scaffolds before soaking in SBF did not feature any precipitates (Fig. 1). After 14 days of immersion in SBF, the surface of foams was covered by precipitates with spongy, cauliflower-like morphology, typical of bone-like apatite crystals. The presence of precipitates was more pronounced for H44-derived samples (Fig. 8c,d) [44].

3.3. In-vitro cell viability

Materials containing carbon nanotubes and reduced graphene oxide demonstrated strong optical absorption in the near-infrared (NIR) region, making them promising materials for use in the photothermal ablation of tumours [11,14–16,19,20]. MK-C and H44-C Biosilicate-C composite foams also showed promising results in this respect [20]. However, serious concerns arise in relation to pharmacokinetics, metabolism and toxicity of carbon-based nanomaterials for biomedical applications [45]. The toxicity of carbon materials remains controversial, because various studies show conflicting results [46,47]. Investigation of the in-vitro cytotoxic effects of the fabricated Biosilicate-C composite foams is thus essential for assessing their suitability for further use.

Fig. 9 shows the comparative viability of ST-2 cells, seeded on the surface of foamed samples for 1 and 7 days. The OD values remained well below the OD value of the positive control (+), after 1 day. However, an increase in the number of cells was observed with increasing time, indicating cytocompatibility of the tested materials. After 7 days, all samples met the biocompatibility threshold specified in the ISO standard [48], consisting of a number of viable cells exceeding 70% of the control. The ratio of OD values between 7 days and 1 day after cell seeding correlates with cell proliferation [49]. No significant difference between MK-derived (d_7/d_1: 5.93) and H44-derived (d_7/d_1: 5.43) foams was observed. The obtained results also match the cell viability test of commercial Biosilicate® scaffolds that demonstrates the cytocompatibility in terms of proliferation of osteoblast and fibroblast cells [21]. For carbon containing foams, the cell proliferation on H44-C composite foam (d_7/d_1: 9.14) is approximately 1.5 times higher than on MK-C composite foams (d_7/d_1: 6.35). The carbon containing foams also showed better cell proliferation with respect to the foams without carbon. It is therefore possible to assume that the homogeneously distributed carbon phase did not have any negative effect on cell growth, in contrast to previous investigations which showed a negative effect of carbon containing materials on the cell viability [50,51].

The morphology of ST-2 cells, after 1 and 7 days seeding on the MK- and H44-derived foams was observed by fluorescence microscopy after staining with rhodamine phalloidin (for F-actin filaments in red) and DAPI (for nuclei in blue) (Fig. 10). The cells appear well attached on all materials.

3.4. Antibacterial activity

Reports from the literature emphasized that the adhesion of bacteria and biofilm formation can be controlled by surface properties and composition of the adopted biomaterials [19,52,53]. Silicate bio-ceramics such as forsterite, diopside, wollastonite, and åkermanite are reported to possess antibacterial activity against *S. aureus, S. epidermidis* and *E. coli* [52,53]. The antibacterial effect is attributed to exchange of alkali ions by protons from the aqueous medium resulting in the formation of hydroxyl ions, and leading to increased pH values.

Such increased pH values create a micro-environment unsuitable for the growth of bacteria. Consecutive change in the osmotic medium leads to cellular injury [49]. The pH values raised to 9.5 and 9.7 for MK and MK-C samples, respectively; the pH values were 9.9 and 10.5 for analogous samples derived from H44 (Fig. 11). To assess the inherent antibacterial activity of prepared polymer-derived materials, only the MK-derived samples were considered.

The relative bacterial viability of *S. aureus* and *E.coli* on the MK Biosilicate and MK-C Biosilicate C composite foams is shown in Fig. 12. The data were recorded after 3, 6, and 24 h of incubation. A significant and gradual decrease in the relative bacterial viability for both bacterial strains was observed, which confirms the antibacterial activity of tested samples under the investigated conditions. The antibacterial activity results are interesting, as no antimicrobial elements such as silver or gallium were present in the polymer-derived foams prepared in this work.

4. Conclusions

In-vitro bioactivity, cytocompatibility and antibacterial activity of MK-C and H44-C Biosilicate-C composite foams were investigated. In-vitro bioactivity test results in SBF solution confirmed HCA and $CaCO_3$ formation after 14 days immersion in SBF. Moreover, cell biology and antibacterial tests on MK, H44 Biosilicate, and MK-C, H44-C Biosilicate-C composite foams indicated cytocompatibility of the ST-2 cell line and a strong antibacterial activity towards *S. Aureus* and *E. Coli* bacteria, respectively.

CRediT authorship contribution statement

Fulden Dogrul: Investigation, Methodology, Writing – original draft. **Qaisar Nawaz:** Investigation, Methodology. **Hamada Elsayed:** Conceptualization, Investigation, Methodology, Writing – original draft. **Liliana Liverani:**Investigation, Methodology, Writing – original draft. **Dušan Galusek:** Conceptualization, Writing – review & editing. **Enrico Bernardo:** Conceptualization, Methodology, Writing – review & editing. **Aldo R. Boccaccini:** Conceptualization, Writing – review & editing.

Declaration of Competing Interest

The authors declare no conflict of interest.

Acknowledgments

This paper is a part of the dissemination activities of project FunGlass. This project has received funding from the European Union's Horizon 2020 research and innovation program under grant agreement No 739566. The financial support of this work by the JECS Trust and by the grants APVV-19–0010 and SAS-MOST JRP 2018/02 are gratefully acknowledged.

References

[1] L. Crisan, B.V. Crisan, S. Bran, F. Onisor, G. Armencea, S. Vacaras, O.P. Lucaciu, I. Mitre, M. Baciut, G. Baciut, C. Dinu, Carbon-based nanomaterials as scaffolds in bone regeneration, Part. Sci. Technol. 38 (2020) 912–921, https://doi.org/10.1080/02726351.2019.1637382.

[2] S. Kargozar, M. Mozafari, S. Hamzehlou, P. Brouki Milan, H. Won Kim, F. Baino, Bone Tissue engineering using human cells: a comprehensive review on recent trends, current prospects, and recommendations, 2018, Appl. Sci. 9 (2019) 174, https://doi.org/10.3390/app9010174.

[3] G. Turnbull, J. Clark, F. Picard, P. Riches, L. Jian, F. Han, B. Li, W. Shu, 3D bioactive composite scaffolds for bone tissue engineering, Bioact. Mater. 3 (2018) 278–314, https://doi.org/10.1016/j.bioactmat.2017.10.001.

[4] A.R. El-Ghannam, Advanced bioceramic composite for bone tissue engineering: Design principles and structure–bioactivity relationship, 1, J. Biomed. Mater. Res A 69 (2004) 490–501, https://doi.org/10.1002/jbm.a.30022.

[5] L.C. Gerhardt, A.R. Boccaccini, Bioactive glass and glass-ceramic Scaffolds for bone tissue engineering, Materials 3 (2010) 3867–3910, https://doi.org/10.3390/ma3073867.

[6] I. Pires, B. Gouveia, J. Rodrigues, R. Fonte, Characterization of sintered hydroxyapatite samples produced by 3D printing, Rapid Prototyp. J. 20 (2014) 413–421, https://doi.org/10.1108/RPJ-05-2012-0050.

[7] Q. Fu, E. Saiz, M.N. Rahaman, A.P. Tomsia, Bioactive glass scaffolds for bone tissue engineering: state of the art and future perspectives, Mat. Sci. Eng. C. Mater. Biol. Appl. 31 (2011) 1245–1256, https://doi.org/10.1016/j.msec.2011.04.022.

[8] M. Tavoni, M. Dapporto, A. Tampieri, S. Sprio, Bioactive calcium phosphate-based composites for bone, Regen., J. Comp. Sci. 5 (2021) 227, https://doi.org/10.3390/jcs5090227.

[9] N. Kamboj, A. Ressler, I. Hussainova, Bioactive ceramic Scaffolds for bone tissue engineering by powder bed selective laser processing: a review, Materials 14 (2021) 5338, https://doi.org/10.3390/ma14185338.

[10] R. Guimarães Ribas, V. Modelski Schatkoski, T.L. do Amaral Montanheiro, B. Rossi Canuto de Menezes, C. Stegemann, D.M. Gonçalves Leite, G. Patrocínio Thim, Current advances in bone tissue engineering concerning ceramic and bioglass scaffolds: a review, Ceram. Int. 45 (2019) 21051–21061, https://doi.org/10.1016/j.ceramint.2019.07.096.

[11] S. Fu, H. Hu, J. Chen, Y. Zhu, S. Zhao, Silicone resin derived larnite/C scaffolds via 3D printing for potential tumor therapy and bone regeneration, Chem. Eng. J. 382 (2020) 122928, https://doi.org/10.1016/j.cej.2019.122928.

[12] M. Bayat, D. Ghaidari, Chapter 5 Nanoparticles and liver cancer, Nano Drug Deliv. Strateg. Treat. Cancers (2021) 119–143, https://doi.org/10.1016/B978-0-12-819793-6.00006-0.

[13] Y. Yang, J. Liu, C. Liang, L. Feng, T. Fu, Z. Dong, Y. Chao, Y. Li, G. Lu, M. Chen, Z. Liu, Nanoscale metal-organic particles with rapid clearance for magnetic resonance imaging-guided photothermal therapy, ACS Nano 10 (2016) 2774–2781, https://doi.org/10.1021/acsnano.5b07882.

[14] G. Nocito, G. Calabrese, S. Forte, S. Petralia, C. Puglisi, M. Campolo, E. Esposito, S. Conoci, Carbon dots as promising tools for cancer diagnosis and therapy, Cancers 13 (2021) 1991, https://doi.org/10.3390/cancers13091991.

[15] L. Liu, Q. Ma, J. Cao, Y. Gao, S. Han, Y. Liang, T. Zhang, Y. Song, Y. Sun, Recent progress of graphene oxide-based multifunctional nanomaterials for cancer treatment, Cancer Nanotechnol. 12 (2021) 18, https://doi.org/10.1186/s12645-021-00087-7.

[16] H. Ma, C. Jiang, D. Zhai, Y. Luo, Y. Chen, F. Lv, Z. Yi, Y. Deng, J. Wang, J. Chang, C. Wu, A Bifunctional biomaterial with photothermal effect for tumor therapy and bone regeneration, Adv. Funct. Mater. 26 (2016) 1197–1208.

[17] A. Zocca, C.M. Gomes, A. Staude, E. Bernardo, J. Günster, P. Colombo, SiOC ceramics with ordered porosity by 3D-printing of a preceramic polymer, J. Mater. Res. 28 (2013) 2243–2252.

[18] P. Colombo, G. Mera, R. Riedel, G.D. Sorarù, Polymer-derived ceramics: 40 years of research and innovation in advanced ceramics, Ceram. Sci. Technol. Appl. 4 (2013) 245–320, https://doi.org/10.1111/j.1551-2916.2010.03876.x.

[19] T. Zhu, M. Zhu, Y. Zhu, Fabrication of forsterite scaffolds with photothermal-induced antibacterial activity by 3D printing and polymer-derived ceramics strategy, Ceram. Int. 46 (2020) 13607–13614, https://doi.org/10.1016/j.ceramint.2020.02.146.

[20] F. Dogrul, S. Bortolin, D. Del Col, N. Dengo, D. Pedron, M. Michalek, H. Elsayed, D. Galusek, E. Bernardo, Polymer-derived Biosilicate-C composite foams: phase development and photothermal effect, J. Eur. Ceram. Soc. 41 (2021) 380–388, https://doi.org/10.1016/j.jeurceramsoc.2021.09.012.

[21] L.L. Hench, R.J. Splinter, W.C. Allen, T.K. Greenlee, Bonding mechanisms at the interface of ceramic prosthetic materials, J. Biomed. Mater. Res. Symp. 2 (1971) 117.

[22] M.C. Crovace, M.T. Souza, C.R. Chinaglia, O. Peitl, E.D. Zanotto, Biosilicate®: a multipurpose, highly bioactive glass-ceramic. In vitro, in vivo and clinical trials, J. Non-Cryst. Sol. 432 (2016) 90–110, https://doi.org/10.1016/j.jnoncrysol.2015.03.022.

[23] O.P. Filho, G.P. LaTorre, L.L. Hench, Effect of crystallization on apatite-layer formation of bioactive glass 45S5, J. Biomed. Mater. Res. 30 (1996) 509.

[24] Q.Z. Chen, I.D. Thompson, A.R. Boccaccini, 45S5 Bioglass®-derived glass–ceramic scaffolds for bone tissue engineering, Biomaterials 27 (2006) 2414–2425, https://doi.org/10.1016/j.biomaterials.2005.11.025.

[25] J. Moura, L.N. Teixeira, C. Ravagnani, O. Peitl, E.D. Zanotto, M.M. Beloti, H. Panzeri, A.L. Rosa, P.T. de Oliveira, In vitro osteogenesis on a highly bioactive glass-ceramic (Biosilicate), J. Biomed. Mater. Res. 82 (2007) 545–557, https://doi.org/10.1002/jbm.a.31165.

[26] H. Elsayed, P. Rebesan, M.C. Crovace, E.D. Zanotto, E. Bernardo, Biosilicate® scaffolds produced by 3D-printing and direct foaming using preceramic polymers, J. Am. Ceram. Soc. 102 (2019) 1010–1020, https://doi.org/10.1111/jace.15948.

[27] F. Dogrul, F.P. Ożóg, M. Michálek, H. Elsayed, D. Galusek, L. Liverani, A. R. Boccaccini, E. Bernardo, Polymer-derived biosilicate®-like glass-ceramics: engineering of formulations and additive manufacturing of three-dimensional Scaffolds, Materials 14 (2021) 5170, https://doi.org/10.3390/ma14185170.

[28] T. Kokubo, H. Takadama, How useful is SBF in predicting in vivo bone bioactivity? Biomaterials 27 (2006) 2907–2915, https://doi.org/10.1016/j.biomaterials.2006.01.017.

[29] M. Scheffler, T. Takahashi, J. Kaschta, H. Muensted, P. Buhler, P. Greil, Pyrolytic decomposition of preceramic organo polysiloxanes, Innovative Processing and Synthesis of Ceramics, Glass, Compos. IV: Ceram. Trans. 115 (2000) 239–250.

[30] A.J. Salinas, M. Vallet-Regi, Bioactive ceramics: from bone grafts to tissue engineering, RSC Adv. 28 (2013) 11116–11131.

[31] A.M.P. Magri, K.R. Fernandes, F.R. Ueno, H.W. Kido, A.C. da Silva, F.J.C. Braga, R. N. Granito, P.Roberto Gabbai-Armelin, A.C.M. Rennó, Osteoconductive properties of two different bioactive glass forms (powder and fiber) combined with collagen, Appl. Surf. Sci. 423 (2017) 557–565, https://doi.org/10.1016/j.apsusc.2017.06.152.

[32] M. Mami, A. Lucas-Girot, H. Oudadesse, R. Dorbez-Sridi, F. Mezahi, E. Dietrich, Investigation of the surface reactivity of a sol–gel derived glass in the ternary system SiO_2–CaO–P_2O_5, Appl. Surf. Sci. 254 (2018) 7386–7393.

[33] M. Schumacher, P. Habibovic, S. van Rijt, Mesoporous bioactive glass composition effects on degradation and bioactivity, Bioact. Mater. 6 (2021) 1921–1931, https://doi.org/10.1016/j.bioactmat.2020.12.007.

[34] M. Mozafari, F. Moztarzadeh, M. Tahriri, Investigation of the physico-chemical reactivity of a mesoporous bioactive SiO_2–CaO–P_2O_5 glass in simulated body fluid, J. Non-Cryst. Solids 356 (2010) 1470–1478.

[35] D.S. Brauer, N. Karpukhina, D. Seah, R.V. Law, R.G. Hill, Fluoride-containing bioactive glasses, Adv. Mater. Res. 39 (2008) 299–304.

[36] Y. Fujita, T. Yamamuro, T. Nakamura, S. Kotani, C. Ohtsuki, The bonding behavior of calcite to bone, J. Biomed. Mater. Res. Vol. 8 (1991) 991–1003.

[37] J. Vuola, H. Göransson, T. Bähling, S. Asko-Seljavaara, Bone marrow induced osteogenesis in hydroxyapatite and calcium carbonate implants, Biomaterials 17 (1996) 1761–1766, https://doi.org/10.1016/0142-9612(95)00351-7.

[38] E. Raynaud, D. Champion, P. Bernache-Assollant, Thomas, Calcium phosphate apatites with variable Ca/P atomic ratio synthesis, characterisation and thermal stability of powders, Biomaterials 23 (2002) 1065–1072, https://doi.org/10.1016/S0142-9612(01)00218-6.

[39] P. Layrolle, A. Ito, T. Tateishi, Sol-gel synthesis of amorphous calcium phosphate and sintering into microporous hydroxyapatite, Bioceram. J. Am. Ceram. Soc. 81 (1996) 1421–1428.

[40] M. Cerruti, C. Morterra, Carbonate formation on bioactive glasses, Langmuir Vol. 20 (2004) 6382–6388.

[41] A. Antonakos, E. Liarokapis, T. Leventouri, Micro-Raman and FTIR studies of synthetic and natural apatites, Biomaterials 28 (2007) 3043–3054, https://doi.org/10.1016/j.biomaterials.2007.02.028.

[42] J.R. Jones, P. Sepulveda, L.L. Hench, Dose-dependent behavior of bioactive glass dissolution, J. Biomed. Mater. Res. 58 (2001) 720–726.

[43] S. Bano, A. Rincon Romero, D.M. Grant, A. Nommeots-Nomm, C. Scotchford, I. Ahmed, T. Hussain, In-vitro cell interaction and apatite forming ability in simulated body fluid of ICIE16 and 13-93 bioactive glass coatings deposited by an emerging suspension high velocity oxy fuel (SHVOF) thermal spray, Surf. Coat. Technol. 407 (2021) 126764, https://doi.org/10.1016/j.surfcoat.2020.126764.

[44] C. Chandra, H.S. Cahyadi, S. Alvin, W. Devina, J.-H. Park, W. Chang, K.Y. Chung, S. K. Kwak, J. Kim, Revealing the sodium storage mechanism in high-temperature-synthesized silicon oxycarbides, Chem. Mater. 32 (2020) 410–423.

[45] R. Garriga, T. Herrero-Continente, M. Palos, V.L. Cebolla, J. Osada, E. Muñoz, M. J. Rodríguez-Yoldi, Toxicity of carbon nanomaterials and their potential application as drug delivery systems: in vitro studies in Caco-2 and MCF-7 cell lines, Nanomaterials 10 (2020) 1611.

[46] K. Kostarelos, A. Bianco, M. Prato, Promises, facts and challenges for carbon nanotubes in imaging and therapeutics, Nat. Nanotechnol. 4 (2009) 627–633.

[47] A.M. Jastrzębska, P. Kurtycz, A.R. Olszyna, Recent advances in graphene family materials toxicity investigations, J. Nanopart. Res. 14 (2012) 1320–1340.

[48] R.F. Wallin, E.F. Arscott, A practical guide to ISO 10993-5: cytotoxicity, Med. Device Diagn. Ind. (1998).

[49] J. Beal, N.G. Farny, T. Haddock-Angelli, et al., Robust estimation of bacterial cell count from optical density, Commun. Biol. 3 (2020) 512, https://doi.org/10.1038/s42003-020-01127-5.

[50] A.P. Francis, T. Devasena, Toxicity of carbon nanotubes: a review, Toxicol. Ind. Health 34 (2018) 200–210, https://doi.org/10.1177/0748233717747472.

[51] X. Yuan, X. Zhang, L. Sun, Y. Wei, X. Wei, Cellular toxicity and immunological effects of carbon-based nanomaterials, Part. Fibre Toxicol. 16 (2019) 18, https://doi.org/10.1186/s12989-019-0299-z.

[52] M.S. Collin, S.K. Venkatraman, S. Mohanaa, S. Sumathia, E.A. Drweesh, M. M. Elnagar, E.S. Mosa, S. Sasikumar, Solution combustion synthesis of functional diopside, akermanite, and merwinite bioceramics: excellent biomineralization, mechanical strength, and antibacterial ability, Mater. Today Commun. 27 (2021) 102365.

[53] S. Hu, C. Ning, Y. Zhou, L. Chen, K. Lin, J. Chang, Antibacterial activity of silicate bioceramics, J. Wuhan. Univ. Technol. Mater. Sci. Ed. 26 (2011) 226–230.